In the present set-up, photons are stored by reflections from two independent Bragg mirrors, that is, the photon pulse length is shorter than the resonator length. We envisage the construction of a Fabry–Perot-type interferometer where the incoming beam would interfere coherently with both crystal slabs. This additional interference would lead to a transmission resonance at least ten times sharper than the natural Bragg line width. Such devices necessitate a gap width of a few Pendellösung periods, that is, a few hundred micrometres (refs 10 and 11). With the development of free electron lasers, pulses on the 100-fs scale will become available–matching these distances perfectly. □

Received 7 September 1999; accepted 20 January 2000.

1. Perman, B. *et al.* Energy transduction on the nanosecond time scale: early structural events in a xanthopsin photocycle. *Science* **279,** 1946–1950 (1998).
2. Rose-Petruck, C. *et al.* Picosecond-milliAngstrom lattice dynamics measured by ultrafast X-ray diffraction. *Nature* **398,** 310–312 (1999).
3. Liss, K. -D., Magerl, A., Hock, R., Waibel, B. & Remhof, A. The investigation of ultrasonic fields by time resolved X-ray diffraction. *Proc. SPIE* **3451,** 117–127 (1998).
4. Bond, W. L., Duguay, M. A. & Rentzepis, P. M. Proposed resonator for an X-ray laser. *Appl. Phys. Lett.* **10,** 216–218 (1967).
5. Ceglio, N. M., Gaines, D. P., Trebes, J. E., London, R. A. & Stearns, D. G. Time-resolved measurement of double pass amplification of soft X-rays. *Appl. Opt.* **27,** 5022–5025 (1988).
6. Deslattes, R. D. X-ray monochromators and resonators from single crystals. *Appl. Phys. Lett.* **12,** 133–135 (1968).
7. Hart, M. Bragg reflection X-ray optics. *Rep. Prog. Phys.* **34,** 435–490 (1971).
8. Kishimoto, S. An avalanche photodiode detector for X-ray timing measurements. *Nucl. Instrum. Methods Phys. Res. A* **309,** 603–605 (1991).
9. Zachariasen, W. H. *Theory of X-Ray diffraction in Crystals* (Wiley, London, 1945).
10. Steyerl, A. & Steinhauser, K.-A. Proposal of a Fabry-Perot-type interferometer for X-rays. *Z. Phys. B* **34, 221–227 (1979).**
11. Caticha, A. & Caticha-Ellis, S. A Fabry-Perot interferometer for hard X-rays. *Phys. Status Solidi A* **119,** 643–654 (1990).

Acknowledgements

We thank the European Synchrotron Radiation Facility crystal laboratory for the preparation of the resonator.

Correspondence and requests for materials should be addressed to K.-D.L. (e-mail: liss@esrf.fr).

Soft-mode hardening in $SrTiO_3$ thin films

A. A. Sirenko*, C. Bernhard†, A. Golnik†, Anna M. Clark*, Jianhua Hao*, Weidong Si* & X. X. Xi*

* *Department of Physics, The Pennsylvania State University, University Park, Pennsylvania 16802,USA*
† *Max-Planck-Institut für Festkörperforschung, Heisenbergstraße 1, D-70569 Stuttgart, Germany*

Understanding the behaviour of the dielectric constant in ferroelectric thin films remains a challenging problem. These ferroelectric materials have high static dielectric constants, and so are important for their applications in high-storage-density capacitor structures such as dynamic random access memory (DRAM)[1]. But the dielectric constant tends to be significantly reduced in thin films, thereby limiting the potential benefit of ferroelectrics for memory devices[2]. Extensive studies have shown that this phenomenon could be caused by a 'dead layer' of very low dielectric constant between the ferroeletric film and the electrode[2,3]. And, although very few direct measurements are in fact available, it has been recognized that the lattice dynamical properties in the thin films should also play a key role in the reduction[2] of the dielectric constant. Here we report far-infrared ellipsometry and low-frequency dielectric measurements in $SrTiO_3$ thin films, which demonstrate that the Lyddane–Sachs–Teller relation between the optical-phonon eigenfrequencies and the dielectric constant is fully maintained, as is the case in the bulk material. This indicates that the dramatic reduction of the dielectric constant is a consequence of a profound change of the lattice dynamical properties, in particular of the reduced softening of its lowest optical-phonon mode. Our results therefore provide a better understanding of the fundamental limitations of the dielectric constant values in ferroelectric thin films.

Phonons are important in the phase transitions in the ferroelectric perovskite titanates $SrTiO_3$ (STO) and $(Ba,Sr)TiO_3$ (BST)[4,5]. As temperature decreases, the eigenfrequency of the lowest optical mode (the soft mode) falls and approaches zero at a critical temperature T_c where a lattice instability leads to a ferroelectric phase transition[6]. The Lyddane–Sachs–Teller (LST) relation for a crystal with N infrared-active optical modes ($N = 3$ for STO) is:

$$\frac{\epsilon(0)}{\epsilon(\infty)} = \prod_j^N \frac{\omega_{\mathrm{LO}j}^2}{\omega_{\mathrm{TO}j}^2}$$

This relates the static dielectric constant, $\epsilon(0)$, and the high-frequency dielectric constant, $\epsilon(\infty)$, to the eigenfrequencies, $\omega_{\mathrm{LO}j}$ and $\omega_{\mathrm{TO}j}$, of the longitudinal (LO) and transverse (TO) optical-phonon modes, respectively. It is generally found that the eigenfrequencies of the higher optical modes exhibit no sizeable variation with temperature. In bulk crystals the LST relation has been proven experimentally, and the dramatic increase of $\epsilon(0)$ is directly related to the soft-mode behaviour. The decrease of the soft-mode eigenfrequency with temperature in bulk STO suggests a T_c of 32 K and causes $\epsilon(0)$ to increase to values above 20,000 (ref. 5), although zero-point quantum fluctuations of Ti ions prevent a ferroelectric phase transition from occurring[7]. For BST, the most commonly used ferroelectric material for DRAM applications, T_c can be adjusted by the Ba/Sr ratio to up to approximately 130 °C and $\epsilon(0)$ can be as high as 15,000 (ref. 8).

This high dielectric constant should allow the production of very compact capacitor structures. In reality, however, much lower values have been reported in thin films. For example, a dielectric constant of 150 was observed for a 24-nm-thick polycrystalline BST film in a DRAM device structure[3], while a value of $\epsilon(0)$ of ~250 was found in an epitaxial 25-nm-thick STO film[9]. A widely accepted

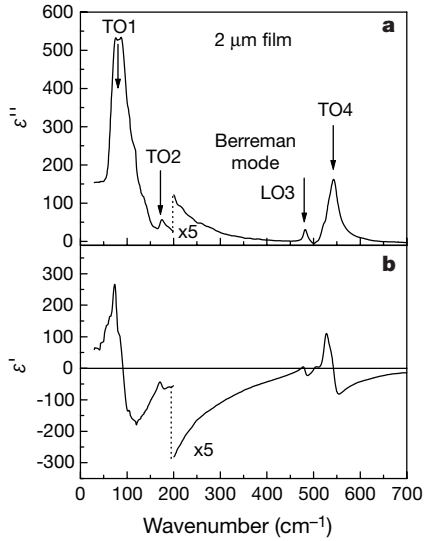

Figure 1 The effective dielectric function for a 2-μm-thick STO film at 200 K. **a,** The real part, $\epsilon'(\omega)$, and **b,** the imaginary parts, $\epsilon''(\omega)$, were measured by FT-IR ellipsometry using synchrotron radiation. From the spectra we determined the eigenfrequencies of the optical phonons by fitting to the factorized form of the dielectric function[5]. The position of the optical phonons obtained from the best fit are marked with arrows.

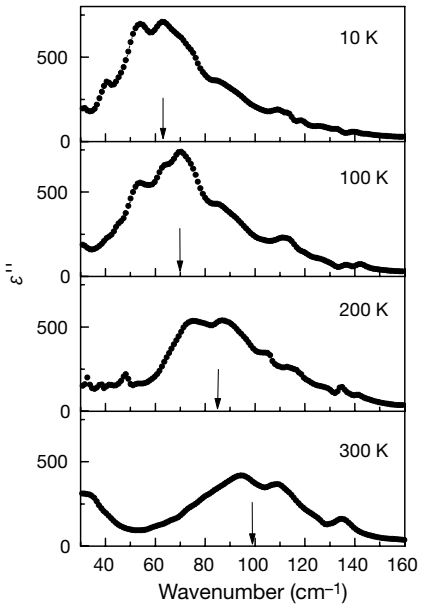

Figure 2 The imaginary part of the effective dielectric function, $\epsilon''(\omega)$, for the 2-μm-thick STO film at different temperatures. The positions of the soft-mode phonon are determined by the best fit to the factorized form of the dielectric function, and are marked with arrows.

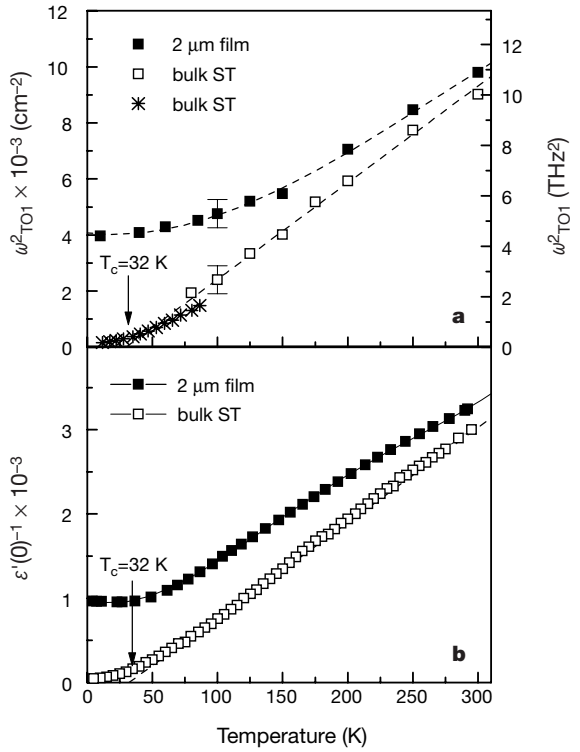

Figure 3 Comparison of the soft-mode frequencies and dielectric constants of bulk and thin-film STO. **a,** The square of the soft-mode TO1 phonon frequency versus temperature for the 2-μm-thick STO film (filled squares) and STO single crystal. The single-crystal data are from our measurement (open squares) and the hyper-Raman result of Vogt[15]; (stars). **b,** The inverse dielectric constant versus temperature for the 2-μm-thick STO film (filled squares) and an STO single crystal (open squares). The hardening of the soft mode in the thin film clearly correlates to a lower static dielectric constant as predicted by the LST relation.

view is that this reduction of $\epsilon(0)$ is caused by a dead layer at the ferroelectric–electrode interface which has a very low dielectric constant[2,3,10]. Such a dead layer may arise from oxygen interdiffusion, chemical reaction, structural defects, Schottky barriers at the interfaces, or the electric-field penetration into the metal electrodes. Using a lattice dynamical approach to consider the interruption of dipole–dipole interaction by the interface, Zhou and Newns further pointed out that this dead-layer effect is intrinsic[2]. Applying the dead-layer model to STO films of various thicknesses, we have derived a temperature-dependent dielectric constant for the volume of the film material which is only about 1,000 at its maximum; that is, still well below the value of $\epsilon(0)$ in bulk single crystals[9]. A fundamental understanding of this effect demands lattice dynamic studies, in particular on the soft-mode behaviour in thin ferroelectric films. An important question in this context is whether or not the LST relation is maintained in the thin films. Because it is rather difficult to measure the optical properties of transparent thin films, there is no report that addresses this issue. Recently, we have used a metal-oxide bilayer Raman scattering technique in STO thin films and observed strong optical-phonon peaks, indicating a lowering of crystal symmetry[11]. However, the soft mode was not detected in the conventional Raman measurements, and an infrared spectroscopic measurement would be more suitable for detecting the infrared-active optical phonons.

We performed the far-infrared ellipsometry measurements at the National Synchrotron Light Source (NSLS) at the Brookhaven National Laboratory. This newly developed technique combines ellipsometry, which directly measures the complex dielectric function without relying on the Kramers–Kronig transformation, with Fourier-transform infrared (FTIR) spectroscopy, which allows a high throughput and multiplexing. Combined with the high brightness of the synchrotron radiation, far-infrared ellipsometry provides a powerful capability to measure vibrational properties with high reliability and accuracy. The experimental set-up and data-processing procedure have been described previously[12]. The complex dielectric function was measured in the frequency range 30–700 cm^{-1} as the temperature was varied from 5 to 300 K. The samples were prepared by pulsed laser deposition with the same bilayer structure as those used in the metal-oxide bilayer Raman scattering experiments[11]. During the deposition, the substrate was heated to 720 °C in an oxygen pressure of 100 mtorr, and the as-deposited film was then cooled to room temperature in 400 torr of oxygen. STO films with thicknesses of 0.5, 1 and 2 μm were deposited on a 0.35-μm conducting oxide $SrRuO_3$ (SRO) buffer layer, which screens the optical signal from the single-crystal STO substrate. The entire bilayer structure was epitaxially grown with high crystalline quality. X-ray diffraction indicated that the STO films have a cubic structure and transform to a tetragonal structure at about 125 K, a slightly higher temperature than in the bulk crystals (~105 K). The static dielectric constant $\epsilon(0)$ was measured at 1 kHz using an LCR meter in a parallel-plate capacitor configuration, formed by evaporating a gold electrode onto the bilayer sample. The low-frequency loss tangent at room temperature is a few times10^{-3} , indicating the high quality of the films.

The real and imaginary parts of the effective dielectric function, $\epsilon'(\omega)$ and $\epsilon''(\omega)$, for the 2-μm-thick STO film at 200 K are shown in Fig. 1. The soft TO1 phonon mode is clearly observed along with other TO modes, and their positions are marked in the figure. We also performed measurements on an SRO buffer layer, and ensured that the substrate signal was indeed blocked by the metallic SRO. The optical response of the SRO film compares very well to the previously reported data[13]. A detailed discussion on the correction procedure for the SRO buffer layer will be published elsewhere. The spectra from the 0.5- and 1-μm STO films showed the same general features as those in Fig. 1, except that the spectral weight of the STO–SRO interface-related Berreman mode[14] decreases with increasing film thickness.

The $\epsilon''(\omega)$ spectrum between 30 and 160 cm^{-1}, which includes the peak corresponding to the soft-mode TO1 phonon, is shown as a function of temperature in Fig. 2 for the 2-μm STO film. The TO1

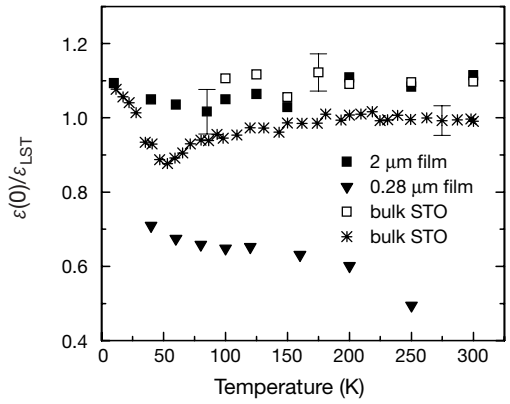

Figure 4 The agreement between the LST relation and the measured $\epsilon(0)$ in 2-μm-thick STO film. The data in Fig. 3 are replotted as the ratio $\epsilon(0)/\epsilon_{LST}$ versus temperature, where $\epsilon(0)$ is the measured value and ϵ_{LST} is the theoretical value based on the LST relation and calculated using the experimental values of the phonon frequencies. The ratio is nearly temperature independent and close to 1 for STO single crystals and the 2-μm film, indicating that the LST relation is maintained with an accuracy of about 10%. The result for a 0.28-μm-thick STO film by Fedorov *et al.*[16] is also included (triangles), which shows a lower and temperature-dependent $\epsilon(0)/\epsilon_{LST}$ ratio because $\epsilon(0)$ is much smaller in the thinner film.

phonon peak is broad due to phonon damping and inhomogeneities in the films. The full-width at half-maximum (FWHM) of the soft mode in the film is about 40 cm^{-1}; this is wider than the 25 cm^{-1} found in bulk crystals[5,15]. The additional broadening is probably the consequence of structural defects in the STO thin film, such as oxygen vacancies[11]. To determine the soft-mode phonon frequency, the experimental spectra are fitted to the factorized form of the dielectric function that takes into account the contribution of the phonon broadening[5]. The positions of the soft mode from the best fit are marked by the arrows in Fig. 2. As shown in this figure, the eigenfrequency of the soft mode decreases as the temperature is lowered. But in clear contrast to the bulk crystals—where the eigenfrequency of the TO1 phonon mode saturates at 13 cm^{-1} at low temperature[15]— in our STO thin film the TO1 eigenfrequency remains fairly high and saturates at 62 cm^{-1}. The eigenfrequencies of the other LO and TO phonon modes are rather similar in the thin film and the single crystals.

To compare our results with the theoretical prediction based on the LST relation, Fig. 3 shows the temperature dependence of the square of the soft-mode frequency, ω^2_{TO1}, and the inverse dielectric constant, $1/\epsilon(0)$, as obtained from the low-frequency dielectric measurement for the STO film and an STO single crystal. The soft-mode frequency data for the single crystal are from our ellipsometric measurement and the hyper-Raman result by Vogt[15]. At room temperature, the values of ω^2_{TO1} are about the same for the thin film and the single crystal, but when the temperature is lowered the softening of the TO1 mode is much weaker in the thin film. Because the eigenfrequencies of all the other LO and TO phonons change only slightly with temperature and are the same as those in the bulk STO, according to the LST relation $\epsilon(0)$ should depend mostly on the eigenfrequency of the soft TO1 mode. Such a trend is indeed observed: the harder soft mode in the thin film clearly correlates to a lower static dielectric constant. In Fig. 4, the ratio of the measured $\epsilon(0)$ to the theoretical value ϵ_{LST}, calculated according to equation (1) with the experimental phonon frequencies and the parameter $\epsilon(\infty) = 5.6$ (ref. 16), is plotted as a function of temperature. In the entire temperature range $\epsilon(0)/\epsilon_{LST}$ remains almost constant and close to 1 for the STO crystal and the 2-μm films. (The slight deviation from 1 at low temperatures is due to the soft-mode splitting into the A_{2u} and E_u symmetry components. Averaged soft-mode frequencies are used in Fig. 4. The low-temperature-film values are obtained with the help of our recent electric-field-induced Raman scattering measurement[22]. This demonstrates that, as in the bulk crystal, the LST relation between the measured eigenfrequencies of the optical-phonon modes and the static dielectric constant is maintained with an accuracy of better than 10% in our 2-μm STO thin films.

We have previously shown that the dead layer correction to $\epsilon(0)$ is negligibly small for 2-μm-thick STO films[9]. The large STO film thickness is central to the observed agreement with the LST relation. Also shown in Fig. 4 is the $\epsilon(0)/\epsilon_{LST}$ ratio for a 0.28-μm-thick STO film obtained by Fedorov *et al.*[16]. Although a similar soft-mode hardening behaviour was obtained by a far-infrared transmittance experiment, the LST relation was not fulfilled because the measured static dielectric constant was much smaller than in our films. This reconfirms that the $\epsilon(0)$ reduction due to the dead-layer effect is more important for smaller film thickness.

From the LST relation, we obtain

$$\frac{\omega^2_{TO1,film}}{\omega^2_{TO1,bulk}} = \frac{\epsilon_{bulk}(0)}{\epsilon_{film}(0)}$$

where $\omega_{TO1,film}$ and $\omega_{TO1,bulk}$ denote the eigenfrequencies of the soft TO1 mode in the thin film and the bulk crystal, respectively. Our result confirms this relation, and suggests that besides the dead-layer effect, the lower dielectric constant in STO thin films is due to their fundamental lattice dynamical properties—specifically, the soft-mode hardening. The physical mechanisms for the soft-mode hardening now become the central issue. It is rather surprising that our highly crystalline thick film exhibits soft-mode behaviour similar to that shown by the very thin, polycrystalline film investigated by Fedorov *et al.*[16], which seems to suggest a mechanism related to the reduced dimensionality. On the other hand, it has been shown that much higher dielectric constants can be obtained in STO films[17,18] and that the epitaxial growth mode has a marked influence on their dielectric properties[18], which suggests a critical role of strain and defects. An analysis of our recent electric-field-induced Raman scattering results in STO thin films indicates that the local polar regions surrounding the oxygen vacancies contribute to the soft-mode hardening.

Our result has implications for the theories of dielectric response in ferroelectric thin films. The phenomenological theory that attributes the reduction of permittivity to the interface-modified depolarization field[19] should be reconciled with the soft-mode behaviour in thin films. It also shows that the microscopic theory of the intrinsic dead-layer effect[2] needs to be modified to extend it beyond the soft-mode hardening in the interfacial layer. The result we report here could also be relevant to investigations of other ferroelectric materials, and to the 'size effect' on ferroelectric properties in polycrystalline ceramics. For example, in polycrystalline BST thin films, the reduction of dielectric constant has been attributed to interfacial dead-layer effect, cation nonstoichiometry, and in-plane stress[20]. In fine-grained $BaTiO_3$, the small grain size and stress are closely linked, and cause an increase in the dielectric constant[21]. Such size effects will no doubt influence soft-mode behaviour in thin films and fine particles, with significant implications for high-$\epsilon(0)$ applications of ferroelectric thin films. □

Received 31 August; accepted 20 December 1999.

1. Kotecki, D. E. *et al.* (Ba,Sr)TiO_3 dielectrics for future stacked-capacitor (DRAM). *IBM J. Res. Dev.* **43,** 367–382 (1999).
2. Zhou, C. & Newns, D. M. Intrinsic dead layer effect and the performance of ferroelectric thin film capacitors. *J. Appl. Phys.* **82,** 3081–3088 (1997).
3. Basceri, C. *et al.* The dielectric response as a function of temperature and film thickness of fiber-textured (Ba, Sr)TiO_3 thin films grown by chemical vapor deposition. *J. Appl. Phys.* **82,** 2497–2504 (1997).
4. Shirane, G. & Yamada, Y. Lattice-dynamical study of the 110 °K phase transition in $SrTiO_3$. *Phys. Rev.* **177,** 858–863 (1969).
5. Servoin, J. L. *et al.* Infrared dispersion in $SrTiO_3$ at high temperature. *Phys. Rev. B* **22,** 5501–5506 (1980).

6. Cochran, W. Crystal stability and the theory of ferroelectricity. *Adv. Phys.* **9,** 387 (1960).
7. Müller, K. A. & Burkard, H. $SrTiO_3$: an intrinsic quantum paraelectric below 4 K. *Phys. Rev. B* **19,** 3593–3602 (1979).
8. Mitsui, T. & Nomura, S. in *LANDOLT-BÖRNSTEIN Numerical Data and Functional Relationships in Science and Technology* (eds Hellwege, K. H. & Hellwege, A. M.) Vol. 16(a) 328–359 (Springer, Berlin, 1981).
9. Li, H. C. *et al.* Thickness dependence of dielectric loss in $SrTiO_3$ thin films. *Appl. Phys. Lett.* **73,** 464–466 (1998).
10. Black, C. T. & Welser, J. J. Electric-field penetration into metals: Consequences for high-dielectric-constant capacitors. *IEEE Trans. Electron Devices* **46,** 776–780 (1999).
11. Sirenko, A. A. *et al.* Observation of the first-order Raman scattering in $SrTiO_3$ thin films. *Phys. Rev. Lett.* **82,** 4500–4503 (1999).
12. Henn, R. *et al.* Far infrared ellipsometry using synchrotron radiation: the out-of-plane response of $La_{2-x}Sr_xCuO_4$ thin solid films. **313,** 642–648 (1998).
13. Kostic, P. *et al.* Non-Fermi-liquid behavior of $SrRuO_3$: Evidence from infrared conductivity. *Phys. Rev. Lett.* **81,** 2498–2501 (1998).
14. Berreman, D. W. Infrared absorption at longitudinal optic frequency in cubic crystal films. *Phys. Rev.* **130,** 2193–2198 (1963).
15. Vogt, H. Refined treatment of the model of linearly coupled anharmonic oscillators and its application to the temperature dependence of the zone-center soft-mode frequencies of $KTaO_3$ and $SrTiO_3$. *Phys. Rev. B* **51,** 8046–8059 (1995).
16. Fedorov, I. *et al.* Far-infrared spectroscopy of a $SrTiO_3$ thin film. *Ferroelectrics* **208,** 413–427 (1998).
17. Fuchs, D. *et al.* High dielectric constant and tunability of epitaxial $SrTiO_3$ thin film capacitors. *J. Appl. Phys.* **85,** 7362–7369 (1999).
18. Lippmaa, M. *et al.* Step-flow growth of $SrTiO_3$ thin films with a dielectric constant exceeding 10^4. *Appl. Phys. Lett.* **74,** 3543–3545 (1999).
19. Vendik, O. G. & Ter-Martirosyan, L. T. Size effect in layered structures, ferroelectric/normal metal and ferroelectric/high T_c superconductor. *Sov. Phys. Solid State* **36,** 1778–1781 (1994).
20. Streiffer, S. K. *et al.* Ferroelectricity in thin films: The dielectric response of fiber-textured $(Ba_xSr_{1-x})Ti_{1+y}O_{3+z}$ thin films grown by chemical vapor deposition. *J. Appl. Phys.* **86,** 4565–4575 (1999).
21. Frey, M. H. & Payne, D. A. Grain-size effect on structure and phase transformations for barium titanate. *Phys. Rev. B* **54,** 3158–3168 (1996).
22. Akimov, I. A. *et al.* Electric field-induced soft-mode hardening in $SrTiO_3$ films. *Phys. Rev. Lett.* (submitted).

Acknowledgements

We thank M. Cardona, H. Vogt, L. E. Cross, D. M. Newns, T. M. Shaw, S. B. Desu, J. Humlíček and J. Petzelt for discussions; G. P. Williams and L. Carr for technical support at the U4IR and U12IR beamlines at NSLS at Brookhaven National Laboratory, a US DOE supported user facility; and I. A. Akimov for the Raman scattering measurements. This work was partially supported by the NSF, DOE and DARPA.

Correspondence and requests for materials should be addressed to A.A.S. (e-mail: sirenko@phys.psu.edu).

Extended surface chirality from supramolecular assemblies of adsorbed chiral molecules

M. Ortega Lorenzo*, C. J. Baddeley*, C. Muryn*† & R. Raval*

** Leverhulme Centre for Innovative Catalysis and Surface Science Centre, Department of Chemistry, University of Liverpool, Liverpool L69 7ZD, UK*

The increasing demand of the chemical and pharmaceutical industries for enantiomerically pure compounds has spurred the development of a range of so-called 'chiral technologies' (ref. 1), which aim to exert the ultimate control over a chemical reaction by directing its enantioselectivity[2]. Heterogeneous enantioselective catalysis[3–5] is particularly attractive because it allows the production and ready separation of large quantities of chiral product while using only small quantities of catalyst. Heterogeneous enantioselectivity is usually induced by adsorbing chiral molecules onto catalytically active surfaces[1,3–7]. A mimic of one such catalyst is formed by adsorbing (*R*,*R*)-tartaric acid molecules on Cu(110) surfaces: this generates a variety of surface phases, of which only one is potentially catalytically active[8], and leaves the question of how adsorbed chiral molecules give rise to enantioselectivity. Here we show that the active phase consists of extended supramolecular assemblies of adsorbed (*R*,*R*)-tartaric acid, which destroy existing symmetry elements of the underlying metal and directly bestow chirality to the modified surface. The adsorbed assemblies create chiral 'channels' exposing bare metal atoms, and it is these chiral spaces that we believe to be responsible for imparting enantioselectivity, by forcing the orientation of reactant molecules docking onto catalytically active metal sites. Our findings demonstrate that it is possible to sustain a single chiral domain across an extended surface—provided that reflection domains of opposite handedness are removed by a rigid and chiral local adsorption geometry, and that inequivalent rotation domains are removed by successful matching of the rotational symmetry of the adsorbed molecule with that of the underlying metal surface.

The hydrogenation of β-ketoesters over Ni catalysts that have been modified with (*R*,*R*)-tartaric acid ((*R*,*R*)-TA) is one the most successful heterogeneous enantioselective reactions, producing enantiomeric excesses of >90% of the hydrogenated *R*-product[4,6,7]. The enantioselectivity can be switched to yield the *S*-enantiomer product by simply using the mirror-image (*S*,*S*)-tartaric acid as a modifier[6]. When a single molecular layer of (*R*,*R*)-tartaric acid is adsorbed on Cu(110), only the ordered phase created at low coverages and temperatures in excess of 350 K is capable of subsequent adsorption of the reactant molecule, methylacetoacetate, which represents the simplest β-ketoester. Surface infrared data[8] indicate that this active phase consists solely of the bitartrate form in which both acid groups have deprotonated to yield carboxylate moieties. The bitartrate molecule straddles the Cu rows so that both carboxylate ends are positioned above the preferred[9] two-fold short-bridge adsorption site, and the oxygen atoms are equidistant from the surface[8] (Fig. 1A). This adsorption mode leaves the C2–C3 bond almost parallel to the surface, with the C–OH groups extending out from the molecular skeleton, projecting a large component parallel to the surface.

Here we present a detailed study of the two-dimensional ordering of this active phase, which gives rise to a low-energy electron diffraction (LEED) pattern (Fig. 1B) that can be indexed in matrix notation as (9 0, 1 2) (see Fig. 1B legend for details of this nomenclature). Scanning transmission microscopy (STM) images of this phase (Fig. 1C) confirm the presence of long-range order, yielding an oblique (9 0, 1 2) repeat surface unit mesh, with the dimensions (Å) 23.04×7.68 , $\alpha = 19.47°$. Each unit cell contains three molecules, resulting in a fractional coverage of 1/6 with respect to the number density of surface metal atoms. The STM images reveal that the bitartrate molecules are self-assembled in rows of three, each row stacking in parallel with others to form long chains. These long chains are aligned along the $\langle 1\bar{1}4 \rangle$ surface direction, which does not coincide with any of the symmetry directions present on the Cu(110) surface. As a result, this molecular growth direction has the effect of destroying all the symmetry elements of the underlying metal, leading directly to the creation of a chiral surface that is non-superimposable on its mirror image. This observation suggests that cooperative[10] behaviour of the adsorbed bitartrate molecules plays a central role in bestowing chirality, or 'handedness', to the achiral metal surface. We attribute this self-assembly to the close proximity of the α-hydroxy groups on neighbouring bitartrate molecules, leading to intermolecular hydrogen-bonding interactions that extend across the surface. The growth direction of this supramolecular assembly is dictated solely by the conformation of the α-hydroxy groups on the adsorbed bitartrate species (Fig. 1A); in this case, the optimum interaction leads to a $\langle 1\bar{1}4 \rangle$ chain alignment. We note that in order to restrict supramolecular growth along one particular direction, the locations of the hydroxy groups need to be constrained in space. The bitartrate form meets this requirement by its two-point attachment

† Permanent address: IRC for Surface Science, University of Manchester, Manchester M13 9PL, UK.